Engineering Phosphinate-Containing Rhodamines for Turn-On Photoacoustic Imaging Applications

Frederik Brøndsted,[a] Yuan Fang,[a] Xinqi Zhou,[b,c] and Cliff I. Stains[a,d,e,*]

[a]Department of Chemistry, University of Virginia, Charlottesville, VA 22904, USA

[b]Department of Chemistry, University of Nebraska-Lincoln, Lincoln, NE 68588, USA

[c]Current Address: Department of Chemistry, University of California, Berkeley, CA 94720, USA

[d]University of Virginia Cancer Center, University of Virginia, Charlottesville, VA 22908, USA

[e]Virginia Drug Discovery Consortium, Blacksburg, VA 24061, USA

*E-mail: cstains@virginia.edu

Abstract

Photoacoustic imaging (PAI) is an emerging imaging technique with applications in preclinical and point-of-care settings. PAI is a light-in, sound-out technique which uses pulsed laser excitation with near-infrared (NIR) light to elicit local temperature increases through non-radiative relaxation events, ultimately leading to the production of ultrasound waves. The classical xanthene dye scaffold has found numerous applications in fluorescence imaging, however, xanthenes are rarely utilized for PAI since they do not typically display NIR absorbance. Herein, we report the ability of Nebraska Red (**NR**) dyes to produce photoacoustic (PA) signal and provide a rational design approach to reduce the hydrolysis rate of ester containing dyes. By converting a relatively hydrolytically labile phosphinate ester to a more stable thiophosphinate ester, we were able to reduce the rate of ester hydrolysis 3.6-fold within a new dye, termed **SNR_{700}**. Leveraging the stabilized NIR absorbance of this dye, we were able to construct the first rhodamine-based, turn-on PAI imaging probe for hypochlorous acid (HOCl) that is compatible with commercial PA instrumentation. This probe, termed **SNR_{700}-HOCl**, has a limit of detection of 500 nM for HOCl and is capable of producing contrast up to 2.9 cm deep in tissues using PAI. This work provides a new set of rhodamine-based PAI agents as well as a rational design approach to stabilize esterified versions of **NR** dyes with desirable properties for PAI. In the long term, the reagents described herein could be utilized to enable non-invasive imaging of HOCl in disease-relevant model systems.

Introduction

PAI is a promising imaging modality for preclinical research and point-of-care applications.[1-3] Commercial PAI instruments utilize pulsed NIR lasers capable of exciting dyes with absorbance in the 680 – 980 nm range.[4-6] PA signal is generated through non-radiative relaxation leading to cycles of thermoelastic expansion events that give rise to pressure waves which can be detected by ultrasound transducers.[7] This photoacoustic effect was first described by Alexander Graham Bell in 1880.[8] Given that biological tissues are 1000-fold more transparent to sound compared to light, imaging depths in the cm range can be achieved by PAI.[7, 9] Furthermore, PAI is an attractive alternative to deep-tissue imaging techniques such as magnetic resonance imaging (MRI), X-ray computed tomography (CT), and positron emission tomography (PET) due to its relatively low cost and lack of ionizing radiation. Nonetheless, PAI is currently limited by the lack of diversity of small molecule scaffolds capable of producing PA readouts, which in turn, limits the ability to generate PA probes for biologically relevant analytes.

The aza-BODIPY,[10-11] hemicyanine,[3, 12-14] and cyanine scaffolds[15] have been the primary small-molecule dyes employed for PAI due to compatibility of their maximal absorbance with commercial PAI instrumentation. Recent chemistry-focused efforts have leveraged activity-based sensing approaches[16-20] to develop turn-on or acoustogenic small molecule PA reporters from these scaffolds.[4-6, 13-14] Such reporters operate through judicious choice of a functional group that selectively reacts with a target analyte and subsequent installation of that functional group on a dye to render it nonabsorbent in the NIR. Upon reaction with the target analyte, a chemical transformation occurs such that the dye becomes NIR absorbent and PA active. This approach has resulted in acoustogenic probes for nitric oxide,[15, 21-22] glutathione,[13] copper,[2] and alkaline phosphatase.[3] However, greater chemical diversity in PA active small molecule dyes is

necessary to expand the toolbox of acoustogenic probe across a broader range of biologically relevant analytes.

Xanthene dyes, typified by rhodamine, rhodol, and fluorescein are historically among the most utilized optical probes and have been extensively studied.[23-27] In particular, spirocyclization at the electrophilic C'9 position of xanthenes with a functional group capable of selectively reacting with a target analyte is a well-established approach for constructing absorbance off-on probes (**Figure 1**).[28-29] Indeed, this spiroring-opening strategy has proven to be generalizable across a wide range of analytes including reactive oxygen and nitrogen species,[16, 30] metal ions,[31] and enzymes.[25] Nonetheless, there are a limited number of examples of xanthene dyes capable of producing PA signal[32-34] since the absorbance of these dyes does not typically fall within the 680 – 980 nm range of commercial PAI instrumentation. Thus, the ability to generate acoustogenic probes has been hindered by the inability to utilize the highly generalizable xanthene spiroring-opening strategy for analyte sensing.

Efforts to red-shift the absorbance of xanthenes have demonstrated that introduction of heteroatom functionalities at the bridging position of xanthenes, such as B,[35-37] C,[38] S,[39-40] Si,[41] Ge,[42] SO_2,[43] and C=O,[44] can lead to a significant red-shift in absorbance. Using this strategy, our lab has recently developed phosphinate-containing rhodamine dyes which we termed Nebraska Red (**NR**) dyes.[45-46] These dyes display ~115 nm red-shifts in absorbance compared to the parent dyes containing oxygen at the bridging position, and can be used for a variety of applications in chemical biology, including construction of absorbance off-on probes.[45-49] We hypothesized that the relatively high extinction coefficient ($\varepsilon > 10^4\ M^{-1}\,cm^{-1}$) and NIR absorbance of these dyes would make them excellent candidates for PAI. Herein, we screen a series of four rhodamine-based **NR** dyes for their ability to generate PA signal. From this initial screen, a phosphinate ester-containing **NR** dye, $\mathbf{NR_{700}}$, that displays relatively rapid hydrolysis under

physiological conditions (pH ~7.4), was identified as a promising lead. In order to stabilize this dye to hydrolysis and extend its lifetime in aqueous solutions, we employed rational design to implement a one atom change. This produced a thiophosphinate **NR** derivative, **SNR_{700}**, with a 3.6-fold increase in stability in aqueous media, while retaining desirable photophysical properties for PAI. We further leveraged this stabilized dye to construct an acoustogenic probe for HOCl, the enzymatic product of myeloperoxidase (MPO), which is a clinically relevant diagnostic marker of acute myeloid leukemia (AML).[50-51] This turn-on PA probe, termed **SNR_{700}-HOCl**, is capable of producing a 12.5-fold increase in PA signal in the presence of HOCl, detecting as little as 500 nM HOCl, and providing contrast at imaging depths up to 2.9 cm in tissue. In the long term, xanthene-based dyes that are compatible with commercial PAI instrumentation could provide valuable tools for construction of acoustogenic reporters for disease relevant analytes.

Results and Discussion

Screening NR Dyes for PA Signal. To determine whether **NR** dyes were capable of producing PA signal, we screened a set of four previously published, rhodamine-based dyes with maximal absorbance ≥ 666 nm (**Figure 2a**).[45] This set of dyes contains pairs of phosphinate and phosphinate ethyl esters with varying molar extinction coefficients and quantum yields. Gratifyingly, we observed PA signal that overlaid well with the absorbance spectra of each dye within this panel (**Figures S1** and **S2**). Within this panel, we observed consistently higher relative PA signal for phosphinate esters (**NR_{700}** and **NR_{744}**) compared to their phosphinate analogues (**NR_{666}** and **NR_{698}**, **Figure 2b** and **c**), even accounting for the 66.3% absorbance of **NR_{666}** at 680 nm (**Figure S2**). Given that **NR_{700}** produced the maximal PA signal in our panel, 45% greater than **NR_{744}** (**Figure 2c**), we chose this dye as a scaffold for creation of an acoustogenic probe. While the phosphinate ethyl ester of **NR_{744}** is resistant to hydrolysis, even when incubated at 37 °C for 48 hrs in the presence of 50% FBS in cell culture media,[47] we have previously shown that **NR_{700}** hydrolyzes on the minutes timescale under physiological conditions to produce **NR_{666}**.[45] In the context of a fluorescent probe, the hydrolysis of **NR_{700}** can be an advantage for facilitating cellular uptake followed by hydrolysis to the brighter cell impermeable **NR_{666}** or by providing a means for gated delivery of cargo in cells with subsequent hydrolysis to **NR_{666}** as a readout of delivery.[45] Unfortunately, as a probe for PAI, hydrolysis of **NR_{700}** to **NR_{666}** is less desirable since this would result in a significant decrease in observable PA signal (**Figure S1**, **NR_{666}** versus **NR_{700}**). Accordingly, we set out to identify a rational design approach that could stabilize the phosphinate ester of **NR_{700}** to hydrolysis while simultaneously maintaining PA signal.

Rational Design of a Stabilized NR Ester-Containing Dye. Based on the work of Rahil and Haake,[52] we hypothesize that hydrolysis of **NR_{700}** to **NR_{666}** occurs through

nucleophilic attack of hydroxide anion at phosphorus (**Figure S3**). Although **NR_{744}** displays dramatically reduced hydrolysis compared to **NR_{700}**, likely due to decreased accessibility of the electrophilic phosphorus center to hydroxide, we chose to pursue an approach that would minimally alter the spectroscopic properties of **NR_{700}** to preserve PA signal. Inspired by the reduced hydrolysis of ATP-γ-S compared to ATP,[53-54] we hypothesized that exchanging the P=O group for a P=S group would significantly decrease hydrolysis of the resulting thiophosphinate without appreciably impacting PA signal generation. To test this hypothesis, we synthesized a thiophosphinate analog of **NR_{700}**, termed **SNR_{700}**, starting from a previously reported **NR_{700}** intermediate (**1**, **Scheme 1**).[45] Treatment with Lawesson's reagent followed by oxidation, yielded the target dye in a concise synthetic route. As hypothesized, **SNR_{700}** retained a strikingly similar absorbance and emission profile (**Figure S4**) as well as photophysical properties (**Figure 3a**) compared to **NR_{700}**. However, installation of the thiophosphinate in **SNR_{700}** led to a dramatic 3.6-fold decrease in the rate of ester hydrolysis compared to **NR_{700}** (**Figure 3b**). Next, we assessed the ability of **SNR_{700}** to produce PA signal. Indeed, **SNR_{700}** retained 82% of the PA intensity of **NR_{700}** (**Figure 4**), making it more intense than **NR_{666}**, **NR_{698}**, and **NR_{744}**. Initial confocal imaging studies also demonstrated that **SNR_{700}** was cell permeable (**Figure S5**). These results confirm the ability to reduce hydrolysis of esters in **NR** dyes with a single atom modification, while maintaining desirable photophysical properties for imaging applications.

Design and Synthesis of an Acoustogenic Probe for HOCl. Having identified a robust, PA active **NR** dye, we set out to leverage the classic spiroring-opening approach from xanthenes[28-29] to generate an acoustogenic probe that would be compatible with commercial PAI instrumentation. As an initial target analyte, we chose HOCl, the enzymatic product of MPO. Importantly, expression of MPO is used as a marker for diagnosis of AML in the clinic[50-51] and previous studies have shown that patient-derived

myeloblasts produce stead-state concentrations of 2.4 – 15.6 μM HOCl.[55] Given that expression of MPO and its subsequent production of HOCl is highly restricted to myeloid cells, aberrant HOCl production represents a potentially underutilized diagnostic marker for AML. Thus, we envisioned the development of an acoustogenic **SNR_{700}**-based probe for HOCl. Ultimately, such a probe may provide a non-invasive approach to detecting AML in the clinic relative to bone marrow biopsy. To obtain an **SNR_{700}**-based acoustogenic probe for HOCl, we chose our previously reported **NR-HOCl** sensor, which contains a spirocyclic thioether[56] that selectively reacts with HOCl, as starting point.[45] Using Lawesson's reagent we converted **NR-HOCl** into **SNR_{700}-HOCl** in one step (**Scheme 2**). In the presence of HOCl, we envisioned that **SNR_{700}-HOCl** would oxidize to the corresponding sulfonate, yielding a species displaying NIR absorbance/fluorescence and PA signal. Gratifyingly, the increased hydrolytic stability afforded by the thiophosphinate motif was conserved in **SNR_{700}-HOCl**, which displayed a 3.3-fold slower fluorescence decrease upon reaction with HOCl compared to **NR-HOCl** (**Figure S6**).

***In Vitro* and Cellular Selectivity for HOCl.** Before testing the ability of **SNR_{700}-HOCl** to produce PA signal, we first evaluated the selectivity of **SNR_{700}-HOCl** using fluorescence. *In vitro* examination showed that **SNR_{700}-HOCl** is stable and non-fluorescent in aqueous media, while exhibiting a 280-fold turn-on fluorescence signal in response to HOCl, with peak emission at 734 nm (**Figure 5 and S7**). In addition, **SNR_{700}-HOCl** showed excellent selectivity towards HOCl compared to a panel of reactive oxygen (ROS) and nitrogen (RNS) species consisting of H_2O_2, tert-butyl hydroperoxide, superoxide, •OH, •OtBu, peroxynitrite, and nitric oxide (**Figure S8**), while displaying virtually no cellular toxicity at concentrations relevant to imaging experiments in a luciferase-expressing AML cell line (HL-60-Luc2, **Figure S9**). Encouraged by these findings we evaluated the ability of **SNR_{700}-HOCl** to detect HOCl within living cells. As an initial test, HeLa cells were chosen since they are not known to express MPO. As

expected, we observed no NIR fluorescence in HeLa cells (**Figure 6a**). However, a clear fluorescence turn-on was observed after addition of exogenous HOCl, demonstrating the selectivity of **SNR_{700}-HOCl** (**Figure 6a**). A dose-dependent response to exogenous HOCl addition was also observed in RAW264.7 cells (**Figure S10**). To assess the selectivity of **SNR_{700}-HOCl** for endogenously produced HOCl, we chose the RAW264.7 macrophage cell line which is known to produce HOCl upon stimulation with lipopolysaccharide (LPS) and phorbol 12-myristate 13-acetate (PMA). Upon overnight incubation with LPS (1 μg/mL) followed by 1 hr stimulation with PMA (0.1 μg/mL), we observed a 56% increase in fluorescence relative to untreated cells (**Figure S11**). Lastly, we investigated the ability of **SNR_{700}-HOCl** to detect endogenous HOCl in HL-60-Luc2 cells which have been shown to produce steady-state levels of 1 μM HOCl.[55] Indeed, a clear turn-on fluorescence signal was observed in this AML cell line which decreased by 49% upon addition of an MPO inhibitor, 4-aminobenzoic acid hydrazide (ABAH, **Figure 6b** and **Figure S12**). Taken together, these experiments demonstrate the ability to selectively detect endogenously produced HOCl both *in vitro* and within living cells.

Acoustogenic Detection of HOCl. Having established the ability of **SNR_{700}-HOCl** to selectively detect HOCl within living cells, we next evaluated **SNR_{700}-HOCl** as an acoustogenic probe. Within tissue phantoms, virtually no PA signal was observed from **SNR_{700}-HOCl** prior to addition of HOCl, which induced the formation of a robust PA signal with a peak at 690 nm and a 12.5-fold signal increase over background (**Figure 7a**). Encouraged by these results, we next investigated the limit of detection (LOD) of **SNR_{700}-HOCl** for HOCl using PAI in tissue phantoms. By varying the concentration of HOCl, we observed an LOD by PAI of 500 nM for HOCl (**Figure 7b**). While this LOD was ~100-fold higher compared to the fluorescence LOD of **SNR_{700}-HOCl** for HOCl (**Figure S13**), the PAI LOD is below the range of HOCl measured in patient-derived myeloblasts

(2.4 - 15.6 μM).[55] These data clearly demonstrate the ability to detect HOCl with a turn-on PA signal using **SNR_{700}-HOCl**.

Acoustogenic Imaging of HOCl in Tissues. As a proof-of-concept for deep-tissue imaging with **SNR_{700}-HOCl**, we cut chicken breast cylinders of varying diameters (**Figure S14**) and encased them in a tissue mimicking phantom to facilitate loading onto PAI instrumentation (**Figure S15**). Using this experimental setup, we were able to observe signal from **SNR_{700}-HOCl** stimulated with 100 μM HOCl up to a depth of 2.9 cm in tissue (**Figure 8 and S16**). These results highlight the ability to leverage the spiroring-opening strategy in **NR** dyes to produce acoustogenic probes that are compatible with commercial PAI instrumentation.

Conclusions

In summary, we have demonstrated the ability of **NR** dyes to produce PA signal. Using rational design, we employed a single atom change to reduce the hydrolysis of **SNR_{700}** by 3.6-fold compared to the parent dye. This stabilized dye retains peak absorbance in the NIR for hours, enabling PAI using commercial instrumentation. Further building on this scaffold, we repurposed the well-established spiroring-opening absorbance off-on analyte detection strategy of xanthenes dyes to afford an acoustogenic probe for HOCl, a potential diagnostic marker for AML.[50-51] PA turn-on signal from **SNR_{700}-HOCl** was capable of detecting clinically relevant concentrations of HOCl in tissue phantoms and provided imaging depths up to 2.9 cm in tissues. To the best of our knowledge, **SNR_{700}-HOCl** is the first xanthene-based, acoustogenic probe for HOCl that is compatible with commercial PAI instrumentation. Future efforts in our lab are focused on increasing the signal-to-noise of **NR**-based acoustogenic probes for HOCl and their evaluation in animal models of AML. In a larger context, this work provides design principles for stabilizing **NR** dyes to hydrolysis, providing the community with NIR absorbing xanthenes that can be used for PAI with commercial instrumentation. We expect that the ability to leverage the lexicon of spiroring-opening absorbance off-on strategies of xanthene dyes[28-29] will significantly expand the toolbox of acoustogenic probes for biologically relevant analytes.

Acknowledgements

F. B. was supported by a Mary Anderson Harrison Jefferson Fellowship from the Jefferson Scholars Foundation. The MSOT data included in this study was generated at the Bioimaging and Applied Research Core facility at Virginia Commonwealth University. We thank the Biomolecular Magnetic Resonance Facility, the Hi-Resolution Mass Spectrometer Facility, and we acknowledge the W.M. Keck Center for Cellular Imaging for the usage of the Leica STELLARIS 8 confocal/FLIM/tauSTED microscope system (NIH OD030409). We acknowledge financial support from the NIH (R35GM119751) and the University of Virginia. The content of this work is solely the responsibility of the authors and does not necessarily represent the official views of the NIH.

Conflict of Interest

F. B., Y. F., X. Z., and C. I. S. have filed a patent application on phosphinate-containing dyes.

Associated Content

Supporting figures, experimental and synthetic procedures, and molecular characterization (PDF).

References

(1) Abeyakoon, O.; Woitek, R.; Wallis, M. G.; Moyle, P. L.; Morscher, S.; Dahlhaus, N.; Ford, S. J.; Burton, N. C.; Manavaki, R.; Mendichovszky, I. A.; Joseph, J.; Quiros-Gonzalez, I.; Bohndiek, S. E.; Gilbert, F. J., An optoacoustic imaging feature set to characterise blood vessels surrounding benign and malignant breast lesions. *Photoacoustics* **2022,** *27*, 100383.
(2) Lucero, M. Y.; Tang, Y.; Zhang, C. J.; Su, S.; Forzano, J. A.; Garcia, V.; Huang, X.; Moreno, D.; Chan, J., Activity-based photoacoustic probe for biopsy-free assessment of copper in murine models of Wilson's disease and liver metastasis. *Proc. Natl. Acad. Sci. U. S. A.* **2021,** *118*, e2106943118.
(3) Wu, Y.; Huang, S.; Wang, J.; Sun, L.; Zeng, F.; Wu, S., Activatable probes for diagnosing and positioning liver injury and metastatic tumors by multispectral optoacoustic tomography. *Nat. Commun.* **2018,** *9*, 3983.
(4) Yadav, A. K.; Hernandez, S.; Su, S.; Chan, J., Acoustic-based chemical tools for profiling the tumor microenvironment. *Curr. Opin. Chem. Biol.* **2020,** *57*, 114-121.
(5) Wu, Y.; Zeng, F.; Zhao, Y.; Wu, S., Emerging contrast agents for multispectral optoacoustic imaging and their biomedical applications. *Chem. Soc. Rev.* **2021,** *50*, 7924-7940.
(6) Zhao, Z.; Swartchick, C. B.; Chan, J., Targeted contrast agents and activatable probes for photoacoustic imaging of cancer. *Chem. Soc. Rev.* **2022,** *51*, 829-868.
(7) Wang, L. V.; Hu, S., Photoacoustic tomography: in vivo imaging from organelles to organs. *Science* **2012,** *335*, 1458-1462.
(8) Bell, A. G., On the production and reproduction of sound by light. *American Journal of Science* **1880,** *s3-20*, 305-324.
(9) Wang, L. V.; Yao, J., A practical guide to photoacoustic tomography in the life sciences. *Nat. Methods* **2016,** *13*, 627-638.
(10) Knox, H. J.; Chan, J., Acoustogenic Probes: A New Frontier in Photoacoustic Imaging. *Acc. Chem. Res.* **2018,** *51*, 2897-2905.
(11) Zhou, E. Y.; Knox, H. J.; Liu, C.; Zhao, W.; Chan, J., A Conformationally Restricted Aza-BODIPY Platform for Stimulus-Responsive Probes with Enhanced Photoacoustic Properties. *J. Am. Chem. Soc.* **2019,** *141*, 17601-17609.
(12) Gardner, S. H.; Brady, C. J.; Keeton, C.; Yadav, A. K.; Mallojjala, S. C.; Lucero, M. Y.; Su, S.; Yu, Z.; Hirschi, J. S.; Mirica, L. M.; Chan, J., A General Approach to Convert Hemicyanine Dyes into Highly Optimized Photoacoustic Scaffolds for Analyte Sensing. *Angew. Chem. Int. Ed.* **2021,** *60*, 18860-18866.
(13) Lucero, M. Y.; Chan, J., Photoacoustic imaging of elevated glutathione in models of lung cancer for companion diagnostic applications. *Nat. Chem.* **2021,** *13*, 1248-1256.
(14) Lucero, M. Y.; Gardner, S. H.; Yadav, A. K.; Borri, A.; Zhao, Z.; Chan, J., Activity-based Photoacoustic Probes Reveal Elevated Intestinal MGL and FAAH Activity in a Murine Model of Obesity. *Angew. Chem. Int. Ed.* **2022,** *61*, e202211774.
(15) Lucero, M. Y.; East, A. K.; Reinhardt, C. J.; Sedgwick, A. C.; Su, S.; Lee, M. C.; Chan, J., Development of NIR-II Photoacoustic Probes Tailored for Deep-Tissue Sensing of Nitric Oxide. *J. Am. Chem. Soc.* **2021,** *143*, 7196-7202.
(16) Chan, J.; Dodani, S. C.; Chang, C. J., Reaction-based small-molecule fluorescent probes for chemoselective bioimaging. *Nat. Chem.* **2012,** *4*, 973-84.
(17) Messina, M. S.; Quargnali, G.; Chang, C. J., Activity-Based Sensing for Chemistry-Enabled Biology: Illuminating Principles, Probes, and Prospects for Boronate Reagents for Studying Hydrogen Peroxide. *ACS Bio. Med. Chem. Au* **2022**, *In Press*, DOI: 10.1021/acsbiomedchemau.2c00052.

(18) Bruemmer, K. J.; Crossley, S. W. M.; Chang, C. J., Activity-Based Sensing: A Synthetic Methods Approach for Selective Molecular Imaging and Beyond. *Angew. Chem. Int. Ed.* **2020,** *59*, 13734-13762.
(19) Ohata, J.; Bruemmer, K. J.; Chang, C. J., Activity-Based Sensing Methods for Monitoring the Reactive Carbon Species Carbon Monoxide and Formaldehyde in Living Systems. *Acc. Chem. Res.* **2019,** *52*, 2841-2848.
(20) Aron, A. T.; Reeves, A. G.; Chang, C. J., Activity-based sensing fluorescent probes for iron in biological systems. *Curr. Opin. Chem. Biol.* **2018,** *43*, 113-118.
(21) Reinhardt, C. J.; Zhou, E. Y.; Jorgensen, M. D.; Partipilo, G.; Chan, J., A Ratiometric Acoustogenic Probe for in Vivo Imaging of Endogenous Nitric Oxide. *J. Am. Chem. Soc.* **2018,** *140*, 1011-1018.
(22) Reinhardt, C. J. J.; Xu, R. W.; Chan, J., Nitric oxide imaging in cancer enabled by steric relaxation of a photoacoustic probe platform. *Chem. Sci.* **2020,** *11*, 1587-1592.
(23) Lavis, L. D.; Raines, R. T., Bright ideas for chemical biology. *ACS Chem. Biol.* **2008,** *3*, 142-155.
(24) Lavis, L. D.; Raines, R. T., Bright building blocks for chemical biology. *ACS Chem. Biol.* **2014,** *9*, 855-66.
(25) Lavis, L. D., Teaching Old Dyes New Tricks: Biological Probes Built from Fluoresceins and Rhodamines. *Annu. Rev. Biochem.* **2017,** *86*, 825-843.
(26) Lavis, L. D., Live and Let Dye. *Biochemistry* **2021,** *60*, 3539-3546.
(27) Grimm, J. B.; Lavis, L. D., Caveat fluorophore: an insiders' guide to small-molecule fluorescent labels. *Nat. Methods* **2022,** *19*, 149-158.
(28) Chen, X.; Pradhan, T.; Wang, F.; Kim, J. S.; Yoon, J., Fluorescent chemosensors based on spiroring-opening of xanthenes and related derivatives. *Chem. Rev.* **2012,** *112*, 1910-56.
(29) Zheng, Q.; Ayala, A. X.; Chung, I.; Weigel, A. V.; Ranjan, A.; Falco, N.; Grimm, J. B.; Tkachuk, A. N.; Wu, C.; Lippincott-Schwartz, J.; Singer, R. H.; Lavis, L. D., Rational Design of Fluorogenic and Spontaneously Blinking Labels for Super-Resolution Imaging. *ACS Cent. Sci.* **2019,** *5*, 1602-1613.
(30) Chen, X.; Tian, X.; Shin, I.; Yoon, J., Fluorescent and luminescent probes for detection of reactive oxygen and nitrogen species. *Chem. Soc. Rev.* **2011,** *40*, 4783-804.
(31) Carter, K. P.; Young, A. M.; Palmer, A. E., Fluorescent sensors for measuring metal ions in living systems. *Chem. Rev.* **2014,** *114*, 4564-601.
(32) Ikeno, T.; Hanaoka, K.; Iwaki, S.; Myochin, T.; Murayama, Y.; Ohde, H.; Komatsu, T.; Ueno, T.; Nagano, T.; Urano, Y., Design and Synthesis of an Activatable Photoacoustic Probe for Hypochlorous Acid. *Anal. Chem.* **2019,** *91*, 9086-9092.
(33) Rathnamalala, C. S. L.; Pino, N. W.; Herring, B. S.; Hooper, M.; Gwaltney, S. R.; Chan, J.; Scott, C. N., Thienylpiperidine Donor NIR Xanthene-Based Dye for Photoacoustic Imaging. *Org. Lett.* **2021,** *23*, 7640-7644.
(34) Zhou, X.; Fang, Y.; Wimalasiri, V.; Stains, C. I.; Miller, E. W., A long-wavelength xanthene dye for photoacoustic imaging. *Chem. Commun.* **2022,** *58*, 11941-11944.
(35) Shimomura, N.; Egawa, Y.; Miki, R.; Fujihara, T.; Ishimaru, Y.; Seki, T., A red fluorophore comprising a borinate-containing xanthene analogue as a polyol sensor. *Org. Biomol. Chem.* **2016,** *14*, 10031-10036.
(36) Zhou, X.; Lesiak, L.; Lai, R.; Beck, J. R.; Zhao, J.; Elowsky, C. G.; Li, H.; Stains, C. I., Chemoselective Alteration of Fluorophore Scaffolds as a Strategy for the Development of Ratiometric Chemodosimeters. *Angew. Chem. Int. Ed.* **2017,** *56*, 4197-4200.
(37) Yin, R.; Fang, Y.; Zhou, X.; Stains, C. I., Synthesis and application of a ratiometric probe for hydrogen peroxide. *Methods Enzymol.* **2020,** *639*, 23-36.
(38) Grimm, J. B.; Sung, A. J.; Legant, W. R.; Hulamm, P.; Matlosz, S. M.; Betzig, E.; Lavis, L. D., Carbofluoresceins and carborhodamines as scaffolds for high-contrast fluorogenic probes. *ACS Chem. Biol.* **2013,** *8*, 1303-10.

(39) Ohulchanskyy, T. Y.; Donnelly, D. J.; Detty, M. R.; Prasad, P. N., Heteroatom substitution induced changes in excited-state photophysics and singlet oxygen generation in chalcogenoxanthylium dyes: Effect of sulfur and selenium substitutions. *J. Phys. Chem. B* **2004,** *108*, 8668-8672.
(40) Detty, M. R.; Prasad, P. N.; Donnelly, D. J.; Ohulchanskyy, T.; Gibson, S. L.; Hilf, R., Synthesis, properties, and photodynamic properties in vitro of heavy-chalcogen analogues of tetramethylrosamine. *Bioorg. Med. Chem.* **2004,** *12*, 2537-2544.
(41) Koide, Y.; Urano, Y.; Hanaoka, K.; Terai, T.; Nagano, T., Development of an Si-rhodamine-based far-red to near-infrared fluorescence probe selective for hypochlorous acid and its applications for biological imaging. *J. Am. Chem. Soc.* **2011,** *133*, 5680-5682.
(42) Koide, Y.; Urano, Y.; Hanaoka, K.; Terai, T.; Nagano, T., Evolution of group 14 rhodamines as platforms for near-infrared fluorescence probes utilizing photoinduced electron transfer. *ACS Chem. Biol.* **2011,** *6*, 600-608.
(43) Liu, J.; Sun, Y. Q.; Zhang, H.; Shi, H.; Shi, Y.; Guo, W., Sulfone-Rhodamines: A New Class of Near-Infrared Fluorescent Dyes for Bioimaging. *ACS Appl. Mater. Interfaces* **2016,** *8*, 22953-22962.
(44) Daly, H. C.; Matikonda, S. S.; Steffens, H. C.; Ruehle, B.; Resch-Genger, U.; Ivanic, J.; Schnermann, M. J., Ketone Incorporation Extends the Emission Properties of the Xanthene Scaffold Beyond 1000 nm. *Photochem. Photobiol.* **2022,** *98*, 325-333.
(45) Zhou, X.; Lai, R.; Beck, J. R.; Li, H.; Stains, C. I., Nebraska Red: a phosphinate-based near-infrared fluorophore scaffold for chemical biology applications. *Chem. Commun.* **2016,** *52*, 12290-12293.
(46) Fang, Y.; Good, G. N.; Zhou, X.; Stains, C. I., Phosphinate-containing rhodol and fluorescein scaffolds for the development of bioprobes. *Chem. Commun.* **2019,** *55*, 5962-5965.
(47) Zhou, X.; Fang, Y.; Lesiak, L.; Stains, C. I., A Phosphinate-Containing Fluorophore Capable of Selectively Inducing Apoptosis in Cancer Cells. *ChemBioChem* **2019,** *20*, 1712-1716.
(48) Lesiak, L.; Zhou, X.; Fang, Y.; Zhao, J.; Beck, J. R.; Stains, C. I., Imaging GPCR internalization using near-infrared Nebraska red-based reagents. *Org. Biomol. Chem.* **2020,** *18*, 2459-2467.
(49) DiMeglio, D.; Zhou, X.; Wirth, T.; Brondsted, F.; Lesiak, L.; Fang, Y.; Shadmehr, M.; Stains, C., Experimentally Calibrated Computational Prediction Enables Accurate Fine-Tuning of Near-Infrared Rhodamines for Multiplexing. *Chemistry* **2022**, DOI: 10.1002/chem.202202861.
(50) Arber, D. A.; Orazi, A.; Hasserjian, R.; Thiele, J.; Borowitz, M. J.; Le Beau, M. M.; Bloomfield, C. D.; Cazzola, M.; Vardiman, J. W., The 2016 revision to the World Health Organization classification of myeloid neoplasms and acute leukemia. *Blood* **2016,** *127*, 2391-405.
(51) Bennett, J. M.; Catovsky, D.; Daniel, M. T.; Flandrin, G.; Galton, D. A.; Gralnick, H. R.; Sultan, C., Proposals for the classification of the acute leukaemias. French-American-British (FAB) co-operative group. *Br. J. Haematol.* **1976,** *33*, 451-458.
(52) Cook, R. D.; Diebert, C. E.; Schwarz, W.; Turley, P. C.; Haake, P., Mechanism of Nucleophilic Displacement at Phosphorus in Alkaline-Hydrolysis of Phosphinate Esters. *J. Am. Chem. Soc.* **1973,** *95*, 8088-8096.
(53) Cox, J. R.; Ramsay, O. B., Mechanisms of Nucleophilic Substitution in Phosphate Esters. *Chem. Rev.* **1964,** *64*, 317-352.
(54) Goody, R. S.; Eckstein, F., Thiophosphate Analogs of Nucleoside Diphosphates and Triphosphates. *J. Am. Chem. Soc.* **1971,** *93*, 6252-6257.
(55) Ozgen, U.; Savasan, S.; Stout, M.; Buck, S.; Ravindranath, Y., Further elucidation of mechanism of resistance to vincristine in myeloid cells: role of hypochlorous acid in degradation of vincristine by myeloperoxidase. *Leukemia* **2000,** *14*, 47-51.

(56) Kenmoku, S.; Urano, Y.; Kojima, H.; Nagano, T., Development of a highly specific rhodamine-based fluorescence probe for hypochlorous acid and its application to real-time imaging of phagocytosis. *J. Am. Chem. Soc.* **2007,** *129*, 7313-7318.

Schemes

Scheme 1. Synthesis of SNR_{700}

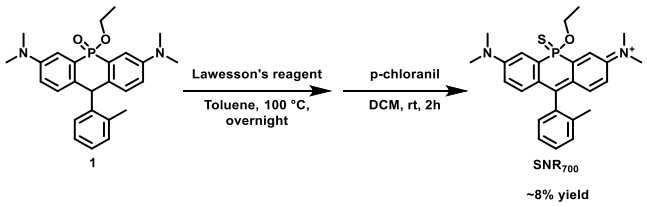

Scheme 2. Synthesis of SNR_{700}-HOCl

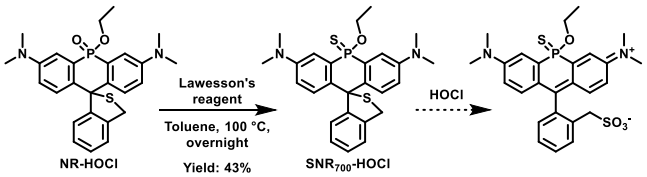

Figures

Figure 1

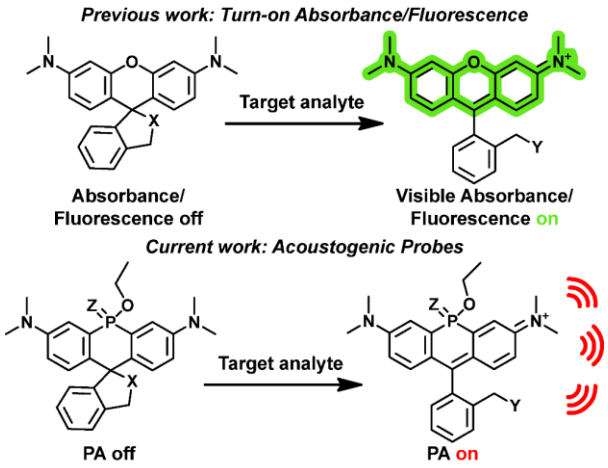

Spiroring-opening at the C'9 position of rhodamine dyes has afforded visible turn-on absorbance/fluorescence probes for a variety of analytes (top). Stabilization of the phosphinate ester in **NR** dyes provides acoustogenic, rhodamine-based probes that are compatible with commercial PAI instrumentation (bottom).

Figure 2

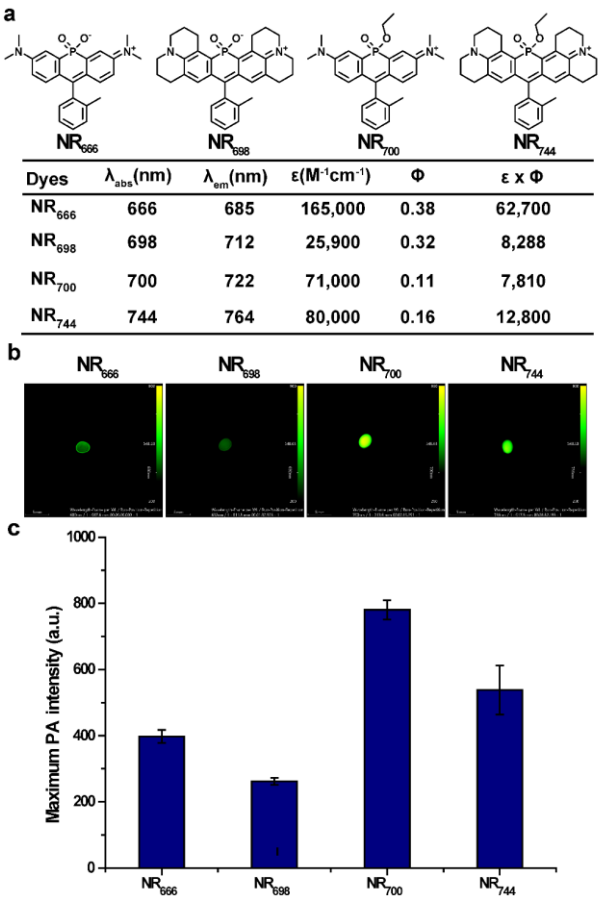

Dyes	λ_{abs}(nm)	λ_{em}(nm)	ε($M^{-1}cm^{-1}$)	Φ	ε x Φ
NR_{666}	666	685	165,000	0.38	62,700
NR_{698}	698	712	25,900	0.32	8,288
NR_{700}	700	722	71,000	0.11	7,810
NR_{744}	744	764	80,000	0.16	12,800

Photoacoustic signal of previously published **NR** dyes. a) Structures of **NR_{666}**, **NR_{700}**, **NR_{698}**, and **NR_{744}** along with their photophysical properties. b) Photoacoustic images of the respective dyes (50 µM) in 1.2 cm thick tissue phantoms. c) Comparison of maximal PA intensities from each dye (see **Figure S1**) (background corrected mean ± SD, n=6).

Figure 3

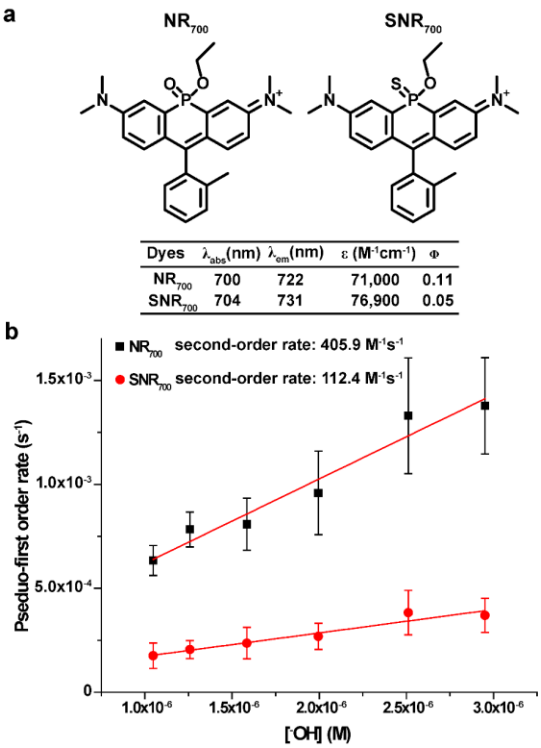

Dyes	λ_{abs}(nm)	λ_{em}(nm)	ε ($M^{-1}cm^{-1}$)	Φ
NR_{700}	700	722	71,000	0.11
SNR_{700}	704	731	76,900	0.05

Incorporation of a thiophosphinate ester significantly reduces ester hydrolysis in **NR** dyes. a) Comparison of **SNR_{700}** and **NR_{700}** photophysical properties. b) Pseudo first-order rates of hydrolysis of **NR_{700}** or **SNR_{700}** at varying concentrations of hydroxide with 100 nM dye (mean ± SD, n=3).

Figure 4

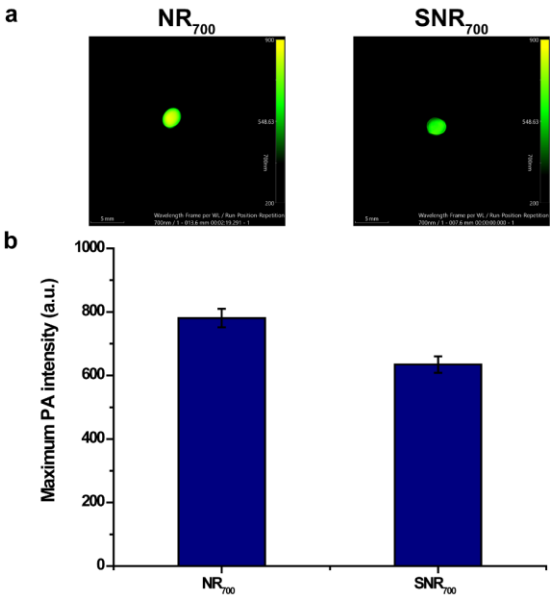

SNR$_{700}$ retains PA signal intensity. a) PA images of 50 µM **NR$_{700}$** and **SNR$_{700}$** in 1.2 cm thick tissue phantoms. b) Quantified PA intensity from panel a (background corrected mean ± SD, n=6).

Figure 5

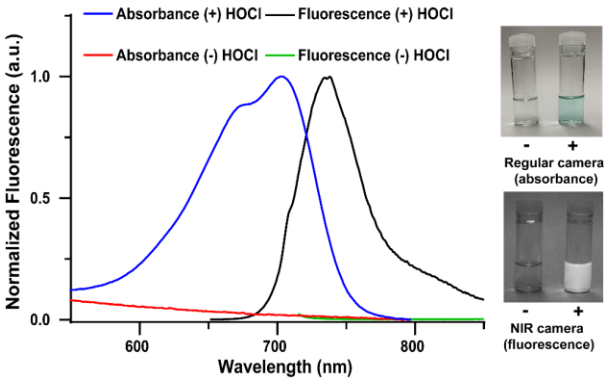

SNR_{700}-HOCl (5 μM) displays a clear absorbance and fluorescence turn-on signal in the presence of 5 μM HOCl. Assays were performed in DPBS (1% DMF). The inset shows absorbance and NIR fluorescence images of samples.

Figure 6

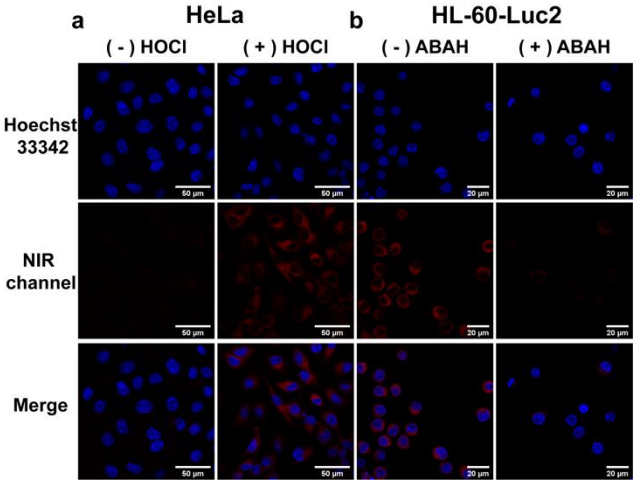

Selective detection of exogenous and endogenous HOCl in living cells with **SNR_{700}-HOCl**. a) Confocal images of HeLa cells incubated with **SNR_{700}-HOCl** (10 µM) before and after the addition of HOCl (20 µM). b) Confocal images of HL-60-Luc2 cells incubated with **SNR_{700}-HOCl** (10 µM) in the absence or presence of the MPO inhibitor ABAH (200 µM).

Figure 7

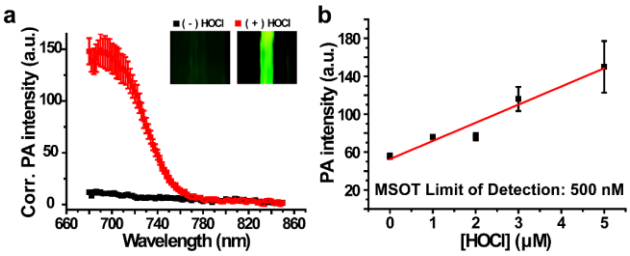

Acoustogenic detection of HOCl using **SNR_{700}-HOCl**. a) **SNR_{700}-HOCl** (25 µM) displays a clear photoacoustic turn-on signal in the presence of 50 µM HOCl (background corrected mean ± SD, n=6). The inset shows PA images of the indicated samples. b) Photoacoustic signal from **SNR_{700}-HOCl** (50 µM) in the presence of the indicated concentration of HOCl (mean ± SD, n=3). All experiments were performed in DPBS (1% DMF) in 1.2 cm thick tissue phantoms.

Figure 8

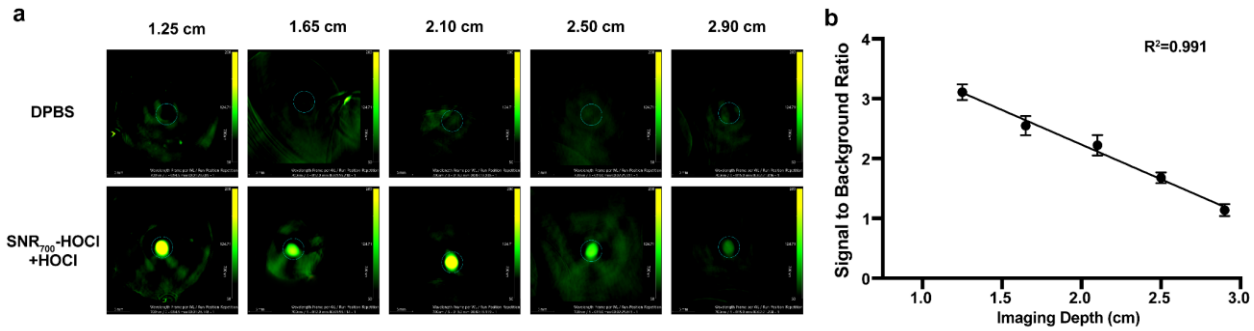

Evaluation of PA imaging depth for **SNR_{700}-HOCl** in tissues. a) PA images of a DPBS blank and 100 μM **SNR_{700}-HOCl** with 100 μM HOCl in chicken breast tissue of the indicated depth. b) Quantified PA signal from panel a (mean ± SD, n=33).

Table of Contents Figure